

Tie-line Power Flow Control Method for Grid-connected Microgrids with SMES Based on Optimization and Fuzzy Logic

Sayed M. Said, Abdelfatah Ali, and Bálint Hartmann

Abstract—In an active distribution grid, renewable energy sources (RESs) such as photovoltaic (PV) and energy storage systems (e. g., superconducting magnetic energy storage (SMES)) can be combined with consumers to compose a microgrid (MG). The high penetration of PV causes high fluctuations of tie-line power flow and highly affects power system operations. This can lead to several technical problems such as voltage fluctuations and excessive power losses. In this paper, a fuzzy logic control based SMES method (FSM) and an optimized fuzzy logic control based SMES method (OFSM) are proposed for minimizing the tie-line power flow. Consequently, the fluctuations and transmission power losses are decreased. In FSM, SMES is used with a robust fuzzy logic controller (FLC) for controlling the tie-line power flow. An optimization model is employed in OFSM to simultaneously optimize the input parameters of the FLC and the reactive power of the voltage source converter (VSC) of SMES. The objective function of minimizing the tie-line power flow is incorporated into the optimization model. Particle swarm optimization (PSO) algorithm is utilized to solve the optimization problem while the constraints of the utility power grid, VSC, and SMES are considered. The simulation results demonstrate the effectiveness and robustness of the proposed methods.

Index Terms—Utility power grid, microgrid, photovoltaic (PV), superconducting magnetic energy storage (SMES), tie-line power, fuzzy logic control (FLC).

I. INTRODUCTION

RECENTLY, renewable energy sources (RESs) are becoming the most important generation power sources. As RESs are environmentally friendly, they have continuously grown worldwide [1], [2]. These sources are interconnected to the distribution systems to supply electricity locally. The electrical microgrid (MG) is the newest structure of the

network that would allow obtaining a better use of distributed energy resources (DERs). This new structure tackles all DERs (e.g., RESs) as a unique subsystem and offers significant control capacities on its operation. This MG can operate as much interconnected to the main utility power grid as autonomously isolated [3], [4]. Therefore, flexible MGs can not only export and import energy to/from the main utility power grid, but also can operate in grid-connected or islanded modes.

Photovoltaic (PV) system is one of the most important types of RESs. Nowadays, grid integration of PV is becoming the most important and fastest-growing form of electricity generation among renewable energies. However, The output power generation of PV has an intermittent nature due to cloud transients [5], [6]. The high penetration of PV can cause several problems such as the fluctuation in tie-line power between the utility power grid and the MG, the voltage rise/dip at point of common coupling (PCC), the violation of power line capability, and the high line power loss. To overcome such problems, energy storage technologies (ESTs) can be utilized in combination with the PV power generation [7], [8] as effective devices with the ability to rapidly and flexibly exchange power with MG. Superconducting magnetic energy storage (SMES) is considered one of the most important EST types where it stores the energy in magnetic form by flowing DC current in the superconducting coil (SC) [9], [10]. The main advantages of SMES devices are the high energy and power density with high conversion efficiency and fast and independent power response in four quadrants. Because of these advantages, SMES is a preferred device in the case of grid-connected MG to overcome the problems resulting from the changing of weather and load power [11].

The combination of SMES and MG with RESs has been pointed out in several research works. Reference [12] studied the power quality improvement of a large-scale PV power generation system and smoothed the power fluctuation under various weather conditions with SMES system. Stabilization of MG which includes PV and wind power generations due to the fluctuation and the faulty condition was achieved by SMES controller considering the state of charge (SOC) and the optimal design of SC, as presented in [13]. In [14], the application of small-scale SMES unit in improving the fault ride-through capability and enhancing the transient behavior of the grid-connected 100 kW PV generation system

Manuscript received: April 29, 2019; accepted: February 11, 2020. Date of CrossCheck: February 11, 2020. Date of online publication: June 25, 2020.

This article is distributed under the terms of the Creative Commons Attribution 4.0 International License (<http://creativecommons.org/licenses/by/4.0/>).

S. M. Said (corresponding author) is with the Department of Electrical Engineering, Aswan University, 81542 Aswan, Egypt, and he is also with the Department of Electric Power Engineering, Budapest University of Technology and Economics, 1111 Budapest, Hungary (e-mail: sayed.said@aswu.edu.eg).

A. Ali is with the Department of Electrical Engineering, South Valley University, 83523 Qena, Egypt (e-mail: a.ahmed@eng.svu.edu.eg).

B. Hartmann is with the Department of Electric Power Engineering, Budapest University of Technology and Economics, 1111 Budapest, Hungary (e-mail: hartmann.balint@vet.bme.hu).

DOI: 10.35833/MPCE.2019.000282



was investigated. A robust SMES controller to stabilize the fluctuation of tie-line power flow for a six-area interconnected power system in the presence of a wind farm was analyzed in [15].

A flat tie-line power of a small wind turbine and a PV array of a grid-connected MG supported by a battery energy storage was proposed in [16]. However, the optimal charging/discharging power of the battery energy storage and the minimization of line power losses were not considered in this work. A linear quadratic-based output regulation approach was suggested in [17] to smooth tie-line power fluctuations with a demand-side control method. This approach was tested and validated by using the modulator aluminum electrolysis load without considering energy storage systems. In [18], an improved droop control strategy was introduced to maintain a constant tie-line power that is suitable for the DC MG by coordinating the designs of droop control characteristics of generators, energy storage units, grid-connected inverter, and a dead band. The SOC and the optimal charging/discharging power of the energy storage units were not included in this study. In [19], a distributed optimal tie-line power

flow control approach was proposed for a multiple-MG system to implement the optimal energy scheduling of each time slot in real time while maintaining the system stability in both grid-connected and islanded modes. In this work, neither the minimization of tie-line power flow nor the reduction of line power losses was considered. The SMES device and its controllability to mitigate the stability of the utility power grid integrated with wind power generation were introduced in [20]. The connection of SMES at different locations was studied to suppress the power fluctuations and to improve the low voltage ride through. In [21], a developed control method was proposed for PV-SMES system based fuzzy control to improve the reliability of MG, eliminate the fluctuating nature of PV generation through local load management, and life extension of DC-link capacitor of voltage source converter (VSC) of SMES due to deep discharging and overcharging operations. The line power losses and the optimally charging/discharging of SMES unit were not considered in this work. A comprehensive comparison of the proposed methods with existing methods in the literature is presented in Table I.

TABLE I
COMPARISON OF PROPOSED METHODS WITH EXISTING METHODS

Method	Methodology	Active and reactive power of storage system	Energy storage reliability	SOC consideration	Minimizing of line power loss
[16]	Battery with a combination of PV and wind generation	Not optimized	Not considered	Not considered	Not considered
[17]	Wind generation units with demand side control method	Not optimized	Not considered	Not considered	Not considered
[18]	Droop control strategy for DC microgrid including energy storage	Not optimized	Not considered	Not considered	Not considered
[19]	Distributed optimal tie-line power flow control for a multiple MG system	Without energy storage	Not considered	Not considered	Not considered
[20]	SMES with wind power generation to improve system stability	Not optimized	Considered	Considered	Not considered
[21]	FLC-based SMES integrated with PV to reduce power fluctuations at PCC	Not optimized	Considered	Considered	Not considered
Proposed FSM	PV and FLC-based SMES to minimize tie-line power and line losses	Simultaneously optimized	Considered	Considered	Considered
Proposed OFSM	PV and optimized FLC-based SMES to minimize tie-line power and line losses	Simultaneously optimized	Considered	Considered	Considered

In this paper, two methods are proposed for minimizing the tie-line power flow between the MG with PV and the utility power grid in the presence of SMES. The first method is fuzzy logic control based SMES method (FSM) and the second method is optimized fuzzy logic control based SMES method (OFSM). The idea of these methods is to simultaneously control/optimize the input parameters of the fuzzy logic controller (FLC) and reactive power of the VSC of SMES to reduce the fluctuation of the tie-line power. The charging/discharging power of the SMES and the reactive power of its VSC are simultaneously computed for mitigating impacts of high power flow between the MG and the utility power grid. The optimal charging/discharging power of the SMES is determined based on the optimal change in the SMES current. A metaheuristic method, i. e., particle swarm optimization (PSO) is used to solve the optimization

model considering the constraints of the utility power grid, VSC, and SMES. In summary, the contributions of this paper are as follows:

- 1) Proposing two methods for minimizing the tie-line power of the MG.
- 2) Defining three indices to study the performance of the proposed methods.
- 3) Considering the reactive power capability of the VSC.
- 4) Considering the power losses in the tie-line.
- 5) Comprehensive simulations are carried out without SMES and with SMES using the proposed methods, respectively.

The remainder of this paper is organized as follows. Section II describes the problems associated with the fluctuation of the tie-line power. The formulation of the proposed FSM and OFSM are given in Section III. Section IV gives a re-

view of the PSO algorithm. The complete solution process is described in Section V. The simulation results are given in Sections VI. Section VII illustrates a comprehensive comparison of the proposed methods and Section VIII draws the conclusions.

II. PROBLEM DESCRIPTION

Due to the intermittent nature of PV power generation and unexpected load variations, the line power at PCC is dramatically changing accordingly [22], [23]. This power transfers between the utility power grid and the PV solar station and it can be negative (i.e., the power goes to the grid) or positive (i.e., the power outgoes from the grid). This power transfer, in turn, dramatically affects the voltage profile of PCC which leads to the release of large reactive power from the grid to regulate the voltage profile at the desired value. Hence, the total losses of the utility power grid will increase, which significantly affects the loadability of transmission lines. The impact of the solar radiation variation and load variation on the tie-line power at PCC is presented in Fig. 1. Therefore, to make the voltage at PCC within limits and reduce the total losses of the transmission lines, the power transfer between the utility power grid and the MG should be minimized as much as possible.

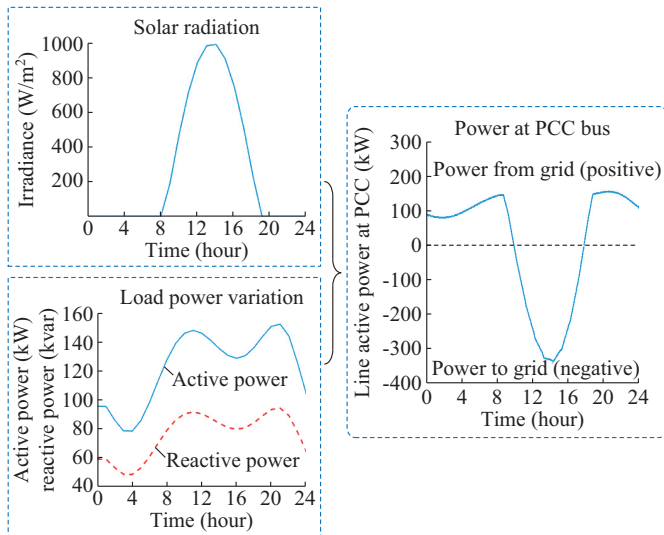


Fig. 1. Detailed problem description due to solar radiation and load power variations.

III. PROPOSED METHODS

A. Description

Two methods are proposed to minimize the power transfer between the utility power grid and the MG. These methods are based on SMES unit, in the presence of PV source, to compensate the required demand load power during the night period in which there is no power generation from PV. Moreover, the SMES stores the extra energy during the day period when the generation power of PV is greater than the demand load power. Figure 2 shows the schematic diagram of the proposed methods.

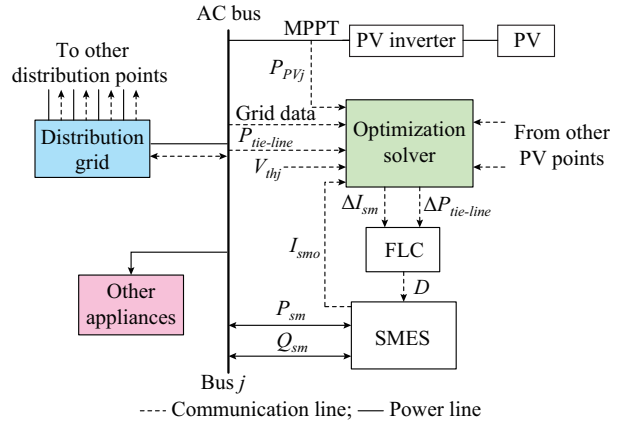


Fig. 2. Detailed diagram of proposed methods.

As shown in the Fig. 2, there are five signals applied to the optimization solver, PV output power P_{PVj} , the data of distribution grid, the active power transfer at a common point $P_{tie-line}$, the voltage thresholds V_{thj} , and the initial current of the SMES I_{smo} . The output signals from the optimization solver are the variation of transferred power $\Delta P_{tie-line}$ (i.e., the difference between generation power of PV P_{PV} and demand load power P_l) and the variation of SMES current ΔI_{sm} (i.e., the difference between the reference and actual SMES currents). The two output signals are applied to the FLC for generating the optimal duty cycle value D which is compared with the sawtooth signal and produces the gating signal to the DC-DC chopper circuit. The chopper circuit is responsible for the active power flow of SMES P_{sm} between the SC and the AC grid. Q_{sm} is the reactive power flow of SMES. On the other hand, the reactive power at PCC should be injected/absorbed in a cooperative manner between the VSC of SMES and the utility power grid to regulate the voltage at PCC around a specified standard value.

B. FSM

To operate the chopper circuit with a fast response, FLC is employed to set the active power transfer between the SC and the VSC. FLC is considered one of the robust and advanced control techniques which are widely used in power system applications. FLC has several advantages such as: ① simple implementation and use; ② fast response during linear and nonlinear system applications; ③ easy to learn and modify its rules; ④ cheaper in developing compared to other controllers in the same application model [24].

There are four stages to complete the FLC process [25], as shown in Fig. 3. The first stage is the fuzzification stage. In this stage, the numerical input variables are read, measured, and transformed into the appropriate linguistic variables according to corresponding membership function (MF) values. Knowledge base stage introduces the descriptions of the fuzzy MFs represented for each control variable and the necessary rules that define the control objects using linguistic variables. The third stage is interface engine stage which provides the ability to simulate human decision performing and determining the control procedures based on fuzzy logic. Finally, the linguistic variables convert again back to the numerical values in the defuzzification stage. In FSM, two in-

puts $\Delta P_{tie-line}$, ΔI_{sm} and one output D are applied to FLC for producing the pulsating signals to the two switches of DC-DC chopper after comparing with the 1 kHz sawtooth reference signal.

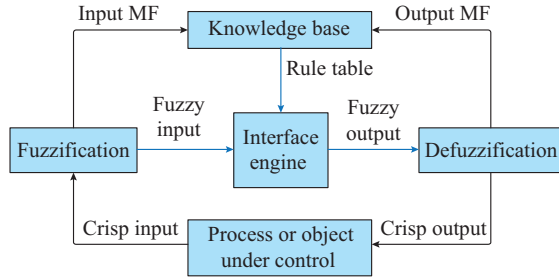
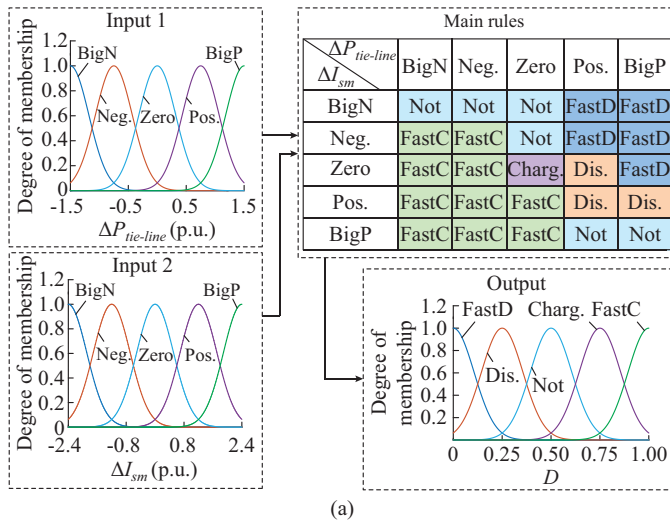
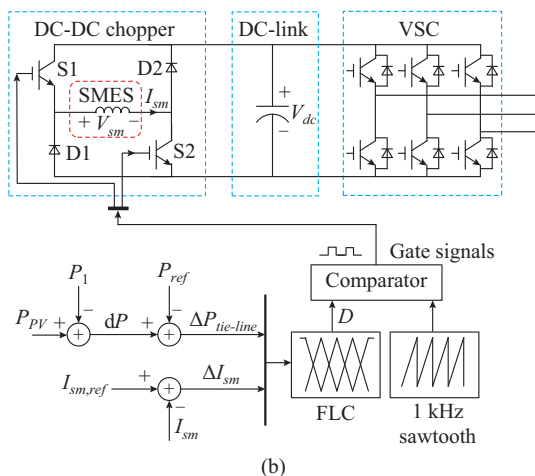


Fig. 3. Main processes of FLC technique.

Gaussian type is used to construct MFs of input and output variables. The rationale behind choosing this type is that it gives better performance for linear and nonlinear applications. The schematic diagram of main rules of FLC and the chopper circuit with FLC are discussed in Fig. 4(a) and (b), respectively, where V_{sm} is the voltage across SC; and V_{dc} is the voltage of DC-link capacitor.



(a)



(b)

Fig. 4. Schematic diagram of main rules of FLC and chopper circuit with FLC. (a) Main rules of FLC. (b) Chopper circuit with FLC.

Graphical user interface (GUI) of MATLAB is used to implement the FLC model. The input and output are fuzzified by five sets on a scale of 0-1 MF degree where BigN, Neg., Zero, Pos., and BigP represent big negative, negative, zero, positive, and big positive for the two input variables, respectively. FastD, Dis., Not, Charg., FastC are denoted to fast-discharge, discharge, no-action, charge, and fast-charge for the output variable, respectively. The equation of Gaussian MF type can be calculated as follows [26]:

$$f(x, \gamma, \varepsilon) = e^{-\frac{(x-\varepsilon)^2}{2\gamma^2}} \quad (1)$$

where x is the input variable; γ is the width of the Gaussian curve; and ε is the center of the peak value.

Defuzzification process can be achieved by IF-AND-THEN routines and the center of gravity method is used to calculate the expected defuzzification process output z_o in the function of membership degree μ_c and the input variable of defuzzification process z as follows [27]:

$$z_o = \frac{\int z\mu_c dz}{\int \mu_c dz} \quad (2)$$

C. OFSM

This method is like the FSM, but the FLC inputs and the injected/absorbed reactive power of the VSC are optimally calculated to minimize the power transfer between the utility power grid and the MG. The main objective function included in the optimization problem is given as follows:

$$\min \sum_{j=1}^{N_{PV}} P_{tie-linej,t}^2 \quad (3)$$

s.t.

$$P_{gj,t} + P_{PVj,t} - P_{Lj,t} \pm P_{smj,t} - V_{j,t} \cdot \sum_{n=1}^{N_B} V_{n,t} (G_{jn} \cos(\delta_{jn,t}) + B_{jn} \sin(\delta_{jn,t})) = 0 \quad \forall j, t \quad (4)$$

$$Q_{gj,t} - Q_{Lj,t} \pm Q_{smj,t} - V_{j,t} \cdot \sum_{n=1}^{N_B} V_{n,t} (G_{jn} \sin(\delta_{jn,t}) - B_{jn} \cos(\delta_{jn,t})) = 0 \quad \forall j, t \quad (5)$$

$$P_{smj}^{\min} \leq P_{smj,t} \leq P_{smj}^{\max} \quad (6)$$

$$\Delta I_{smj}^{\min} \leq \Delta I_{smj,t} \leq \Delta I_{smj}^{\max} \quad (7)$$

$$Q_{smj}^{\min} \leq Q_{smj,t} \leq Q_{smj}^{\max} \quad (8)$$

$$V_j^{\min} \leq V_{j,t} \leq V_j^{\max} \quad (9)$$

$$\begin{cases} S_{smj,t} = \sqrt{P_{smj,t}^2 + Q_{smj,t}^2} \\ S_{smj}^{\min} \leq S_{smj,t} \leq S_{smj}^{\max} \end{cases} \quad (10)$$

where $P_{tie-linej,t}$ is the active power at a common point at bus j ; $P_{gj,t}$ is the active power generation at bus j ; $P_{PVj,t}$ is the active power of PV at bus j ; N_{PV} is the number of PV units; $P_{Lj,t}$ is the active power demand at bus j ; $Q_{gj,t}$ is the reactive power generation at bus j ; $Q_{smj,t}$ is the reactive power of SMES inverter at bus j ; $P_{smj,t}$ is the active power of SMES at bus j ; $Q_{Lj,t}$ is the demand reactive power at bus j ; G_{jn} is the conductance between bus j and bus n ; B_{jn} is the susceptance

between bus j and bus n ; $\delta_{j,n,t}$ is the difference voltage angles at bus j and bus n ; $V_{n,t}$ and $V_{j,t}$ are the voltages at bus n and bus j , respectively; the subscripts min and max represent the minimum and maximum values of corresponding variables, respectively; I_{sm} is the current of SMES; and N_b is the number of buses.

PSO is used in this paper to solve this optimization problem in which the control variables are the reactive power of VSC Q_{sm} of the SMES and the change of current of SMES ΔI_{sm} .

D. PV Model

The complete PV generation system consists of three parts. The first part is an array which forms with modules connected in series and parallel of Sunpower SPR-305-WHT-U (305 W) panel to determine the appropriate output DC voltage and current. In this study, the PV system comprises of 5 series modules and 330 parallels to generate 500 kW DC power. In the second stage, the DC-boost converter is utilized to get a higher DC voltage, which also takes the maximum allowable power from PV array by using maximum power point tracking (MPPT) of incremental conductance. In the third stage, the voltage source inverter (VSI) is utilized to convert DC voltage to AC voltage before the interconnection with the utility power grid. Also, it keeps the DC voltage across the linked capacitor at a constant setpoint voltage. Proportional-integral (PI) technique is used in VSI control for AC and DC voltages after transformation from the three-phase system to dq reference frame. The synchronization between the grid and the output voltage of VSI is achieved by phase-locked loop (PLL) [28]. Incremental conductance control for boost converter [29] and complete VSI control technique are discussed in Fig. 5, where PWM stands for pulse width modulation. The parameters of the complete PV system and its controller are given in Appendix A Table AI.

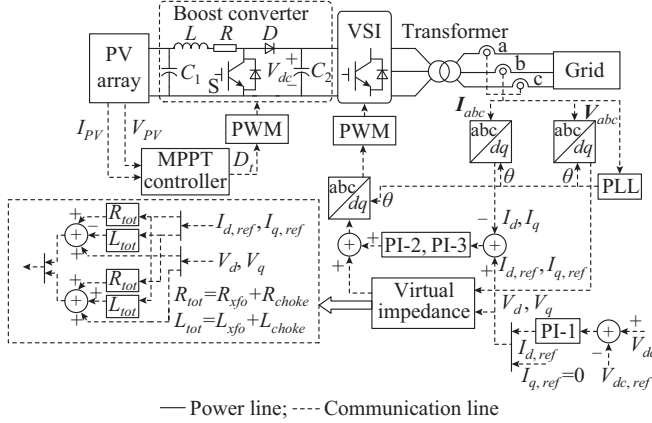


Fig. 5. PV system and its MPPT and VSI controllers.

E. SMES Model

Among all of ESTs, SMES has played an important role in power system applications. SMES stores its energy in magnetic form by flowing a DC through SC which forms from superconductive material with no resistance at its superconducting state [30]. It is cooled with liquid helium or nitrogen (liquid helium for low temperature and liquid nitro-

gen for high temperature), to maintain the temperature of SC lower than or equal to the specific critical temperature T_c of the superconducting material [31], [32].

Figure 6 shows the construction of SMES unit. It consists of a SC with a cooling and protection system, a DC-DC chopper circuit, a bidirectional VSC, a LC filter for AC side, and a three-phase coupling transformer. The chopper circuit is controlled with the proposed FLC which can successfully and fastly set the real power of SMES in the charging, discharging, and standby operation modes. The complete details of the bi-directional VSC are given in [33]. The parameters of the SMES system are listed in Appendix A Table AII.

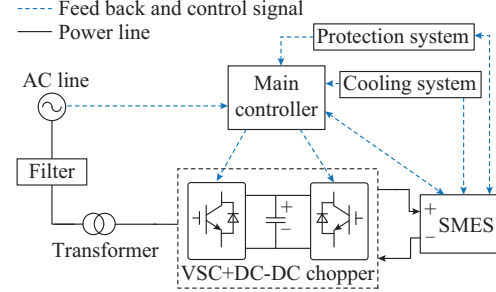


Fig. 6. Complete structure of SMES unit.

The initial energy and operation energy of SMES (E_{smo} and E_{sm}) can be calculated as functions of current of SMES I_{sm} , inductance of SC L_{sm} , P_{sm} , I_{smo} , V_{sm} , as presented in the following equations [34].

$$E_{smo} = \frac{1}{2} L_{sm} I_{smo}^2 \quad (11)$$

$$E_{sm} = \int P_{sm} dt + E_{smo} \quad (12)$$

$$P_{sm} = V_{sm} I_{sm} \quad (13)$$

The voltage across SC is given in (14) in terms of D of the chopper circuit and V_{dc} , as follows:

$$V_{sm} = V_{dc} (2D - 1) \quad (14)$$

The SOC of the SMES can be updated as follows:

$$SOC_t = SOC_{t-1} + \alpha_t \eta_{ch} P_{sm, ch, t} \Delta t - \frac{\sigma_t P_{sm, disc, t} \Delta t}{\eta_{disc}} \quad (15)$$

where η_{ch} and η_{disc} are the charging and discharging efficiencies, respectively; $P_{sm, ch, t}$ and $P_{sm, disc, t}$ are the charging and discharging power of SMES at time t , respectively; and α_t and σ_t are the binary variables ($\alpha_t, \sigma_t \in \{0, 1\}$), and $\alpha_t \sigma_t = 0$ because the charging and discharging of SMES cannot be simultaneously performed.

IV. PSO ALGORITHM

PSO is one of the smart optimization techniques that has been used in many applications. It was first introduced in [35]. PSO is a population-based technique in which these populations are called swarms. Each possible solution of the problem is represented by a particle. The particles move around in a multidimensional search space. Each particle comprises the information of the intended control variable and adapts its position. By moving the particles and evaluat-

ing the fitness function of the new position, PSO can find the optimal solution.

Consider that the position of a particle i at time instant t is $x_i(t)$ while its velocity is $v_i(t)$. The vectors of the position and velocity are stored during algorithm processing at time instant t to be used for updating the population at the next time instant $t+1$. For each iteration, each particle is accelerated toward its previous best position $P_i(t)$ and toward the global best position which is found by particle neighborhood $g_i(t)$. During each iteration, the new velocity will be used to update the particle position. The next position is calculated in the search space. This process will be repeated for a number of iterations until a minimum error is achieved [36]. The position and velocity of the particle at each iteration are computed by [37]:

$$v_i(t+1) = k \left[\omega v_i(t) + C_1 r_1 (P_i(t) - x_i(t)) + C_2 r_2 (g_i(t) - x_i(t)) \right] \quad (16)$$

$$x_i(t+1) = x_i(t) + v_i(t+1) \quad (17)$$

$$\begin{cases} k = 2 / \left| 2 - \phi - \sqrt{\phi^2 - 4\phi} \right| \\ \phi = C_1 + C_2 \\ \phi > 4 \end{cases} \quad (18)$$

where k is the constriction factor; ω is the inertia weight parameter; and r_1 and r_2 are random number between 0 and 1.

To improve the performance of PSO, there is a common approach which promotes a balance between local and global searches. In this approach, ω starts with a high value and during the execution of PSO, it should decrease as follows:

$$\omega = \frac{\omega_{\max} - \omega_{\min}}{iter_{\max}} (iter_{\max} - iter) + \omega_{\min} \quad (19)$$

where ω_{\max} and ω_{\min} are the maximum and minimum inertia weights, respectively; $iter$ is the current iteration; and $iter_{\max}$ is the maximum number of iterations. Normally, ω can be changed between 0.4 and 0.9 [37]. C_1 and C_2 can be computed as follows:

$$C_1 = \frac{C_{1f} - C_{1i}}{iter_{\max}} iter_{\max} + C_{1i} \quad (20)$$

$$C_2 = \frac{C_{2f} - C_{2i}}{iter_{\max}} iter_{\max} + C_{2i} \quad (21)$$

where C_{1i} and C_{2i} are the initial cognitive and social coefficients, respectively; and C_{1f} and C_{2f} are the final cognitive and social coefficients, respectively.

V. SOLUTION PROCESS

The flowchart of FSM and OFSM is shown in Fig. 7. As shown in the figure, at each time instant t , the demand load, PV power, and the status of SMES (e.g., capacity, SOC) are read. Based on the chosen method (FSM or OFSM), the required active power and reactive power from the SMES are calculated to minimize the tie-line power between the PV solar station and the utility power grid (P_{sm} and Q_{sm}) as follows:

1) If the chosen method is FSM, the active and reactive power will be calculated without considering the optimization option.

tion option.

2) If the chosen method is OFSM, the active and reactive power will be calculated considering the optimization option, i.e., the reactive power and FLC inputs are optimally calculated using (3)-(10).

3) Based on the calculated active power (charging/discharging), the SOC of the SMES is updated using (15). The commands generated at time instant t are saved and transmitted over the distribution network. This process is repeated for all time instants.

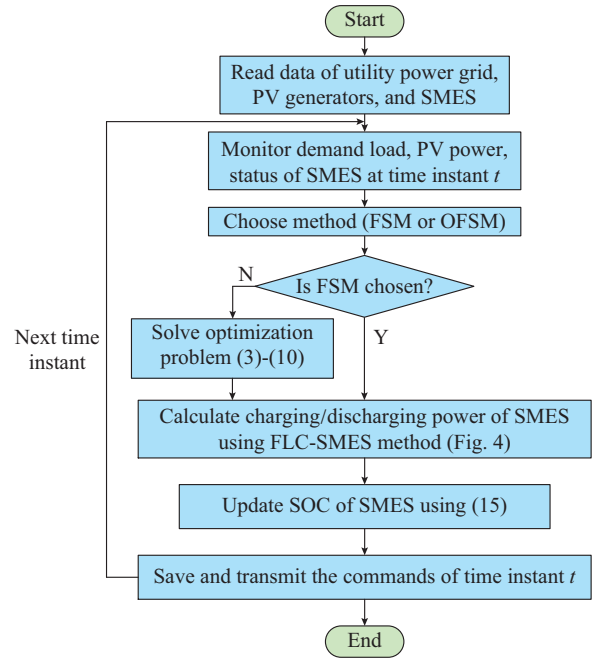


Fig. 7. Flowchart of proposed methods.

VI. SIMULATION RESULTS AND ANALYSIS

The grid-connected PV-SMES MG shown in Fig. 8 has been used as a case study to test the proposed methods.

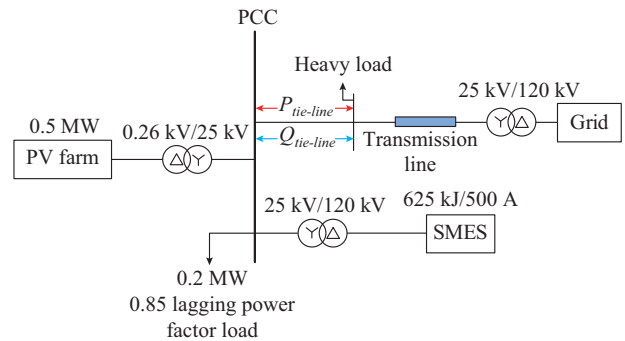


Fig. 8. Grid-connected PV-SMES MG.

The complete data of the utility power grid is shown in Appendix A Table AIII. In this work, three cases are studied to demonstrate the effectiveness of the proposed methods as follows:

- 1) Case 1: the performance of the selected grid is evaluated without using SMES and this is the default base case.
- 2) Case 2: the impact of the FSM on the grid is verified.

3) Case 3: OFSM is used to minimize the tie-line power transfer between the utility power grid and the MG during the whole day.

Figure 9(a) and (b) presents the response of active power at PCC during the day and the total power loss in the transmission line, respectively. It is clear from Fig. 9(a) that by applying the proposed methods, the active power transfer between the utility power grid and the MG due to weather condition and random load demand variation is minimized. It is clear from Fig. 9(b) that the power loss of the transmission line is significantly reduced in cases 2 and 3 compared with case 1. It is worth to mention that the power loss in case 1 is smaller than that in case 2 during the period of 10:00 to 17:00 because of the PV generation during this period is higher than the local load. This means that surplus power will be injected to the heavy load and subsequently the power flow of tie-line from the grid to feed the heavy load will decrease. The best reduction of power loss is achieved by OFSM where the input parameters of FLC and reactive power of VSC are optimally computed to minimize the power flow of tie-line. Therefore, this method is highly recommended to be used for minimizing the power flow of tie-line.

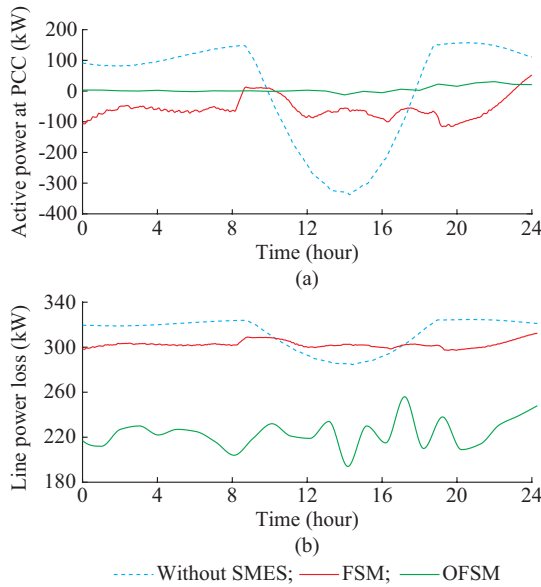


Fig. 9. Response of active power and power loss of transmission line for three cases. (a) Active power of transmission line at PCC bus. (b) Power loss of transmission line.

The voltage profile at PCC and the response of output power of SMES are discussed in Figs. 10 and 11, respectively. The voltage at PCC drops to 0.955 p.u. in case 1 while it is improved in cases 2 and 3. In case 2, the voltage is approximately constant at 1.0 p.u. by absorbing fixed reactive power that is shared between VSC and the power grid without coordination. On the contrary, in case 3, the reactive power of VSC is optimally adjusted with the optimization technique to minimize the transfer power and to keep the voltage at PCC within limit considering the boundary of output power of VSC. Additionally, it is also clear from Fig. 11 that the output power of VSC is calculated optimally to reduce the injected reactive power from power grid at PCC,

which in turn, minimizes the line power loss and regulates the voltage at PCC within the acceptable limit.

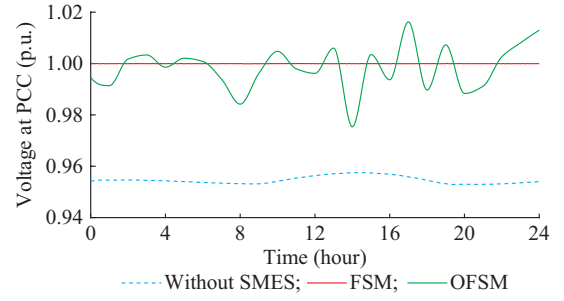


Fig. 10. Profile of voltage at PCC for three cases.

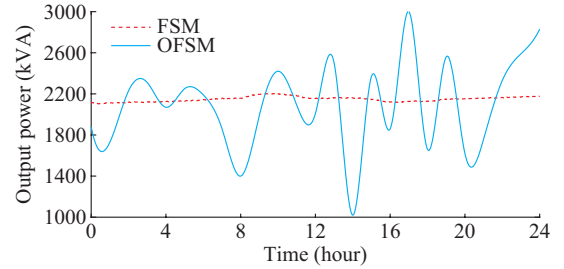


Fig. 11. Response of output power of SMES in proposed methods.

Figure 12(a)-(c) presents the response of duty cycle of chopper circuit, active power of SMES, and current of SC, respectively, in both two proposed methods.

Duty cycle changes between charging and discharging modes when its value is less than 0.5 and larger than 0.5, respectively, within 0 to 1 scale, and it changes optimally in the case of OFSM. The active power of SMES is negative when the power transfers from SMES to PCC, while it is positive in charging mode as the extra active power is stored in SC. In both two proposed methods, the current of SC increases and decreases during charging and discharging events to face the system requirements from load demand and PV power generation, respectively.

Figure 13 shows the voltage of the DC-link capacitor. The voltage is approximately fixed at 2400 V, which in turn validates the effectiveness and robustness of the controller in both two proposed methods.

VII. DISCUSSIONS

The enhancements of the proposed methods for minimizing tie-line power, reducing line energy loss, and regulating voltage at PCC are compared in Tables II and III.

The criteria used to calculate improvement percentage (*IP*) in overshoot/undershoot can be described as follows:

$$IP = \left| \frac{Sh_{base} - Sh_{pro}}{Sh_{base}} \right| \times 100\% \quad (22)$$

where Sh_{base} is the maximum overshoot/minimum undershoot for the base case; and Sh_{pro} is the maximum overshoot/minimum undershoot in the proposed methods.

Tables IV and V illustrate the validation and robustness of the proposed methods in terms of the deviation of the duty cycle and the deviation of the voltage of DC-link capacitor.

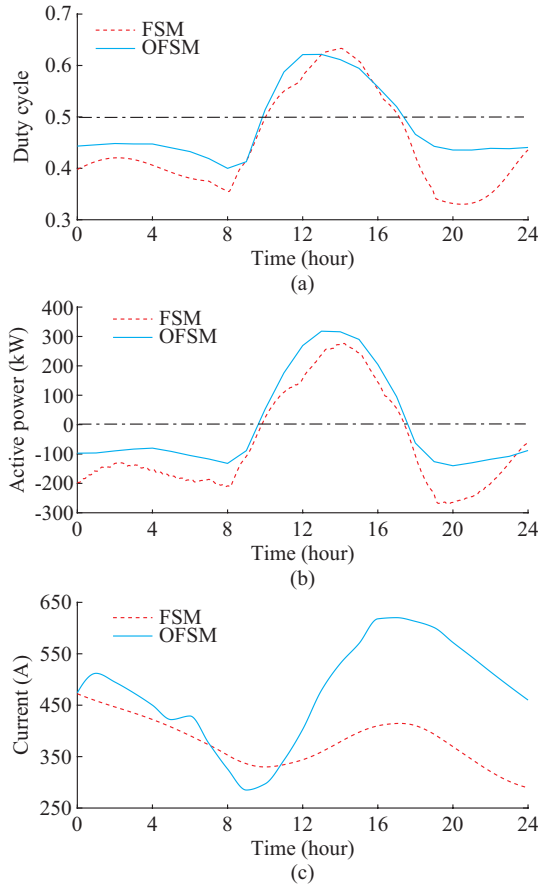


Fig. 12. Response of SMES system. (a) Duty cycle of chopper circuit. (b) Active power of SMES. (c) Current of SC.

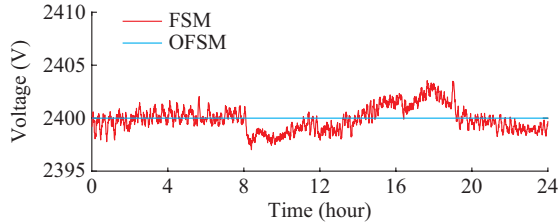


Fig. 13. Response of voltage of DC-link capacitor.

TABLE II
RESULTS OF TIE-LINE POWER, VOLTAGE AT PCC, AND LINE ENERGY LOSS OF HYBRID POWER GENERATION SYSTEM WITH PROPOSED METHODS

Method	Tie-line power (kW)		Line energy loss (MWh)	Average value of voltage at PCC (p.u.)
	Maximum overshoot	Minimum undershoot		
Without SMES	157.20	-377.60	7.50	0.955
FSM	52.35	-115.80	7.26	1.000
OFSM	30.64	-12.51	5.36	0.998

The deviation of the duty cycle of chopper circuit DDC can be calculated according to (23), and the deviation of the voltage of DC-link capacitor VD can be calculated according to (24).

TABLE III
IMPROVEMENTS OF TIE-LINE POWER, VOLTAGE AT PCC, AND LINE ENERGY LOSS OF HYBRID POWER GENERATION SYSTEM WITH PROPOSED METHODS

Case	Method	IP (%)
Tie-line power	FSM with maximum overshoot	66.70
	FSM with minimum undershoot	69.30
	FSM with maximum overshoot	80.50
	FSM with minimum undershoot	96.70
Line energy loss	FSM	3.20
	OFSM	28.53
Voltage at PCC	FSM	4.50
	OFSM	4.30

TABLE IV
RESULTS OF DUTY CYCLE AND VOLTAGE OF DC-LINK CAPACITOR WITH PROPOSED METHODS

Method	Duty cycle	Voltage of DC-link capacitor (V)
FSM with maximum overshoot	0.6330	2403
FSM with minimum undershoot	0.3300	2397
FSM with maximum overshoot	0.6216	2400
FSM with minimum undershoot	0.4000	400

TABLE V
PERFORMANCE AND VALIDATION OF CONTROLLER IN BOTH TWO PROPOSED METHODS

Method	DDC (%)	VD (%)
FSM with maximum overshoot	26.20	0.125
FSM with minimum undershoot	34.00	0.125
FSM with maximum overshoot	24.32	0
FSM with minimum undershoot	20.00	0

$$DDC = \frac{0.5 - D_{MOS/MUS}}{0.5} \times 100\% \quad (23)$$

$$VD = \frac{2400 - V_{MOS/MUS}}{2400} \times 100\% \quad (24)$$

where $D_{MOS/MUS}$ is the maximum overshoot/minimum undershoot value of D ; and $V_{MOS/MUS}$ is the maximum overshoot/minimum undershoot value of the voltage of capacitor.

To demonstrate the robustness of the proposed methods, a step-change in load power and solar irradiance is applied as shown in Fig. 14(a)-(c). The step-changes are applied as follows: ① in the period from 1 to 1.5 s, a step-change in load power is applied; ② in the period from 2 to 2.5 s, a step-change in the solar irradiance is applied; ③ in the period from 3 to 3.5 s, a step-change is applied for both load power and solar irradiance, as shown in Fig. 14(a). The responses of voltage at PCC and voltage of DC-link capacitor during these step-changes by applying FSM and OFSM are given in Fig. 14(b) and (c), respectively. It is clear that a smooth operation of voltage at PCC is achieved in both two proposed methods and it is almost constant regardless of the step-change in load power and solar irradiance. Additionally, the fluctuation in voltage of DC-link capacitor is avoided in the

both two proposed methods, which in turn provides a longer lifetime of the DC-link capacitor and preserves the power electronic components from the thermal stress.

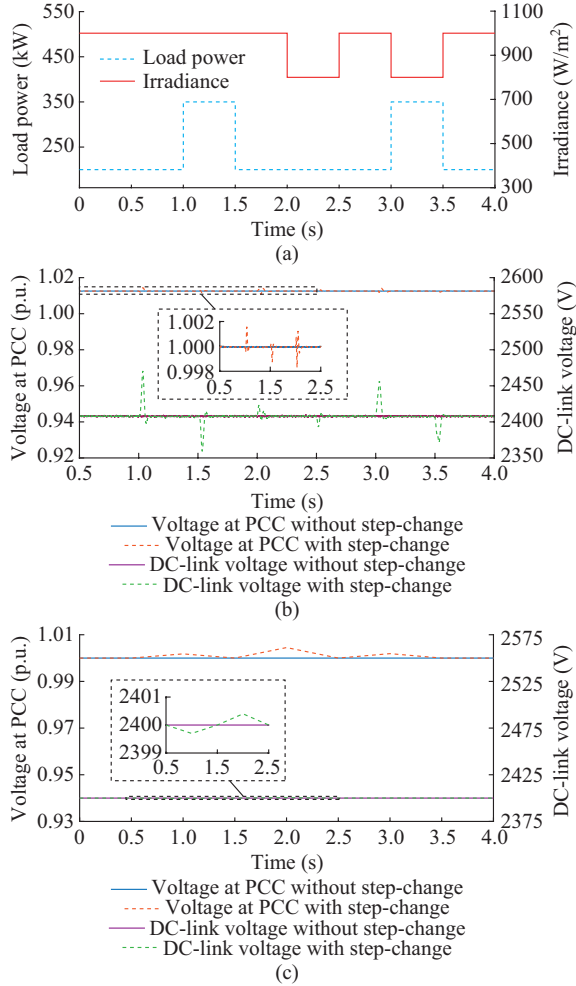


Fig. 14. Response of voltage at PCC and voltage of DC-link capacitor during step-change in load power and solar irradiance in both FSM and OFSM. (a) Step-changes in load power and solar irradiance. (b) FSM. (c) OFSM.

VIII. CONCLUSION

This paper presents two methods, called FSM and OFSM, for minimizing the tie-line power of the MG and regulating the voltage at PCC. The FLC technique is employed in the proposed methods to control the duty cycle of the chopper circuit in SMES. The PSO algorithm is employed to solve the optimization problem considering the constraints of the utility power grid, VSC, and SMES. In the proposed methods, the reactive power of the VSC and the active charging/discharging power of the SMES are optimally and simultaneously computed. Therefore, the tie-line power flow is effectively minimized, and the voltage at PCC is regulated. Furthermore, the fluctuations of tie-line power flow and the transmission power losses significantly decrease. The performance of the proposed methods is compared with the base case without considering SMES. The results demonstrate the effectiveness of the proposed methods for reducing the negative impacts of high tie-line power flow. It is also shown that the optimal coordination between the reactive

power of VSC and the reactive power of utility power grid can perform better in terms of voltage regulation and power loss minimization.

APPENDIX A

TABLE AI
COMPLETE PARAMETERS OF PV SYSTEM AND ITS CONTROLLER

Component	Value
Number of cells per module	96
Open-circuit voltage V_{oc}	64.2 V
Short-circuit current I_{sc}	5.96 A
Operating temperature T_a	25 °C
Cognitive coefficient C_1	400 μ F
Social coefficient C_2	70 mF
Total leakage impedance of transformer (R_{sfo} , L_{sfo})	(0.002 p.u., 0.06 p.u.)
Resistance of choke R_{chock}	0.002 Ω
Reactance of choke L_{chock}	0.00025 H
Nominal voltage of DC bus	1000 V
Switching frequency of VSI	1980 Hz
Switching frequency of MPPT	5 kHz
VSI rated capacity	500 kVA
(K_p, K_i) of V_{DC} controller PI-1	(7, 800)

TABLE AII
PARAMETERS OF SMES SYSTEM

Component	Value
Inductance of SC	5 H
Initial current	500 A
Initial energy	625 kJ
DC-link capacitor	5 mF
Rated capacity of transformer	3 MVA
Rated ratio of transformer	1250 V/25 kV
Resistance of transformer	0.001 p.u.
Inductance of transformer	0.03 p.u.
Inductance of AC filter L_f	800 μ H
Capacitance of AC filter C_f	100 μ F

TABLE AIII
DATA OF UTILITY POWER GRID

Component	Value
Rated capacity of transformer	47 MVA
Rated ratio of transformer	120 kV/25 kV
Resistance of transformer	0.003 p.u.
Inductance of transformer	0.08 p.u.
Length of transmission line	30 km
Resistance of line R_1, R_0	0.1153 Ω /km, 0.413 Ω /km
Reactance of line L_1, L_0	1.05 mH/km, 3.32 mH/km
Capacitance of line C_1, C_0	11.33 nF/km, 5.01 nF/km
Heavy load	6 MW

REFERENCES

- [1] P. S. Georgilakis, "Technical challenges associated with the integration

- of wind power into power systems," *Renewable and Sustainable Energy Reviews*, vol. 12, no. 3, pp. 852-863, Apr. 2008.
- [2] B. Shyam and P. Kanakasabapathy, "Renewable energy utilization in India - policies, opportunities and challenges," in *Proceedings of 2017 International Conference on Technological Advancements in Power and Energy*, Kollam, India, Dec. 2017, pp. 1-6.
- [3] N. Hatziargyriou, H. Asano, R. Iravani *et al.*, "Microgrids," *IEEE Power and Energy Magazine*, vol. 5, no. 4, pp. 78-94, Jul.-Aug. 2007.
- [4] B. Kroposki, R. Lasseter, T. Ise *et al.*, "Making microgrids work," *IEEE Power and Energy Magazine*, vol. 6, no. 3, pp. 40-53, May-Jun. 2008.
- [5] A. Arshad and M. Lehtonen, "A stochastic assessment of PV hosting capacity enhancement in distribution network utilizing voltage support techniques," *IEEE Access*, vol. 7, pp. 46461-46471, Apr. 2019.
- [6] M.-N. Khurshed, K. M. F. Nadeem, G. Ali *et al.*, "A review of estimating solar photovoltaic cell parameters," in *Proceedings of 2nd International Conference on Computing, Mathematics and Engineering Technologies*, Sukkur, Pakistan, Jan. 2019, pp. 1-6.
- [7] M. Farhadi and O. Mohammed, "Energy storage technologies for high-power applications," *IEEE Transactions on Industry Applications*, vol. 52, no. 3, pp. 1953-1961, May-Jun. 2016.
- [8] V. A. Boicea, "Energy storage technologies: the past and the present," *Proceedings of the IEEE*, vol. 102, no. 11, pp. 1777-1794, Nov. 2014.
- [9] L. Ren, Y. Xu, W. Zuo *et al.*, "Development of a movable HTS SMES system," *IEEE Transactions on Applied Superconductivity*, vol. 25, no. 4, pp. 1-9, Aug. 2015.
- [10] M. Song, J. Shi, Y. Liu *et al.*, "100 kJ/50 kW HTS SMES for micro-grid," *IEEE Transactions on Applied Superconductivity*, vol. 25, no. 3, pp. 1-6, Jun. 2015.
- [11] X. Chen, J. Jin, Y. Xin *et al.*, "Integrated SMES technology for modern power system and future smart grid," *IEEE Transactions on Applied Superconductivity*, vol. 24, no. 5, pp. 1-5, Oct. 2014.
- [12] H. R. Seo, A. R. Kim, M. Park *et al.*, "Power quality enhancement of renewable energy source power network using SMES system," *Physica C: Superconductivity and Its Applications*, vol. 471, no. 21-22, pp. 1409-1412, Nov. 2011.
- [13] I. Ngamroo and S. Vachirasricirikul, "Design of optimal SMES controller considering SOC and robustness for microgrid stabilization," *IEEE Transactions on Applied Superconductivity*, vol. 26, no. 7, pp. 1-5, Oct. 2016.
- [14] L. Chen, H. Chen, J. Yang *et al.*, "Conceptual design and evaluation of an HTS magnet for an SMES used in improving transient performance of a grid-connected PV system," *IEEE Transactions on Applied Superconductivity*, vol. 28, pp. 1-8, Apr. 2018.
- [15] S. Dechanupaprittha, K. Hongesombut, M. Watanabe *et al.*, "Stabilization of tie-line power flow by robust SMES controller for interconnected power system with wind farms," *IEEE Transactions on Applied Superconductivity*, vol. 17, no. 2, pp. 2365-2368, Jun. 2007.
- [16] Z. Xiao, J. M. Guerrero, J. Shuang *et al.*, "Flat tie-line power scheduling control of grid-connected hybrid microgrids," *Applied Energy*, vol. 210, pp. 786-799, Jan. 2018.
- [17] C. Zhang, W. Lin, D. Ke *et al.*, "Smoothing tie-line power fluctuations for industrial microgrids by demand side control: an output regulation approach," *IEEE Transactions on Power Systems*, vol. 34, no. 5, pp. 3716-3728, Sept. 2019.
- [18] Y. Che, J. Zhou, T. Lin *et al.*, "A simplified control method for tie-line power of DC micro-grid," *Energies*, vol. 11, no. 4, pp. 933, Apr. 2018.
- [19] Y. Liu, Y. Li, H. Xin *et al.*, "Distributed optimal tie-line power flow control for multiple interconnected AC microgrids," *IEEE Transactions on Power Systems*, vol. 34, no. 3, pp. 1869-1880, May 2019.
- [20] P. Mukherjee and V. V. Rao, "Superconducting magnetic energy storage for stabilizing grid integrated with wind power generation systems," *Journal of Modern Power Systems and Clean Energy*, vol. 7, no. 2, pp. 400-411, Mar. 2019.
- [21] S. M. Said, M. Aly, B. Hartmann *et al.*, "SMES-based fuzzy logic approach for enhancing the reliability of microgrids equipped with PV generators," *IEEE Access*, vol. 7, pp. 92059-92069, Jul. 2019.
- [22] A. Ali, D. Raisz, and K. Mahmoud, "Sensitivity-based and optimization-based methods for mitigating voltage fluctuation and rise in the presence of PV and PHEVs," *International Transactions on Electrical Energy Systems*, vol. 27, no. 12, pp. 1-19, Nov. 2017.
- [23] A. Ali, D. Raisz, and K. Mahmoud, "Voltage fluctuation smoothing in distribution systems with RES considering degradation and charging plan of EV batteries," *Electric Power Systems Research*, vol. 176, pp. 1-7, Nov. 2019.
- [24] L. A. Zadeh, "Fuzzy sets," *Information and Control*, vol. 8, no. 3, pp. 338-353, Jun. 1965.
- [25] S. M. Said and B. Hartmann, "Alleviation of extremely power and voltage variations caused by wind power and load demand using SMES," *Periodica Polytechnica Electrical Engineering and Computer Science*, vol. 63, no. 3, pp. 134-143, Mar. 2019.
- [26] C. W. de Silva, "Fundamentals of fuzzy logic," in *Intelligent Control*. Boca Raton: CRC Press, 2018, pp. 43-68.
- [27] S. S. Sastry, *Intelligent Control*. Boca Raton: CRC Press, 2018.
- [28] T. Thacker, D. Boroyevich, R. Burgos *et al.*, "Phase-locked loop noise reduction via phase detector implementation for single-phase systems," *IEEE Transactions on Industrial Electronics*, vol. 58, no. 6, pp. 2482-2490, Jun. 2011.
- [29] E. M. Ahmed and M. Shoyama, "Stability study of variable step size incremental conductance/impedance MPPT for PV systems," in *Proceedings of 8th International Conference on Power Electronics*, Jeju, South Korea, May-Jun. 2011, pp. 386-392.
- [30] N. Amaro, J. M. Pina, J. Martins *et al.*, "Integration of SMES devices in power systems - opportunities and challenges," in *Proceedings of 2015 9th International Conference on Compatibility and Power Electronics (CPE)*, Costa da Caparica, Portugal, Jun. 2015, pp. 482-487.
- [31] T. Mito, H. Chikarashi, A. Kawagoe *et al.*, "Summary of a 1 MJ conduction-cooled LTS pulse coil developed for 1 MW, 1 s UPS-SMES," *IEEE Transactions on Applied Superconductivity*, vol. 19, no. 3, pp. 1999-2003, Jun. 2009.
- [32] Y. Li, P. Song, Y. Kang *et al.*, "Design of a 30-K/4-kJ HTS magnet cryocooled with solid nitrogen," *IEEE Transactions on Applied Superconductivity*, vol. 28, no. 4, pp. 1-6, Jun. 2018.
- [33] E. A. Mohamed, S. M. Said, B. Hartmann *et al.*, "An efficient fuzzy logic controlled-smes for isolated-microgrid system considering high wind power penetration," in *Proceedings of 2018 5th International Conference on Electric Power and Energy Conversion Systems (EPECS)*, Kitakyushu, Japan, Apr. 2018, pp. 1-6.
- [34] D. Sutanto and K. W. E. Cheng, "Superconducting magnetic energy storage systems for power system applications," in *Proceedings of 2009 International Conference on Applied Superconductivity and Electromagnetic Devices*, Chengdu, China, Sept. 2009, pp. 377-380.
- [35] Eberhart R. and J. Kennedy, "A new optimizer using particle swarm theory," in *Proceedings of the 6th International Symposium on Micro Machine and Human Science*, Nagoya, Japan, Oct. 1995, pp. 39-43.
- [36] M. Settles, "An introduction to particle swarm optimization," Ph.D. dissertation, Department of Computer Science, University of Idaho, Moscow, Russia, 2005.
- [37] A. L. G. Nogueira, L. S. M. Castellanos, E. E. S. Lora *et al.*, "Optimum design of a hybrid diesel-ORC/photovoltaic system using PSO: case study for the city of Cujubim, Brazil," *Energy*, vol. 142, Jan. 2018, pp. 33-45.

Sayed M. Said received the B.Sc. and M.Sc. degrees in electrical engineering from Aswan University, Aswan, Egypt, in 2006 and 2014, respectively. He started work as a research assistant at the Electrical Engineering Department, Aswan University, Aswan, Egypt, since 2010. He is currently working toward the Ph.D. degree at the Doctoral School of Electrical Engineering, Faculty of Electrical Engineering and Informatics, Budapest University of Technology and Economics, Budapest, Hungary. His current research is focused on the integration of wind/PV based on SMES to grid. His interests include power system analysis, renewable energies, power system control and protection, and wind energy with superconducting magnetic energy storage (SMES).

Abdelfatah Ali received the B.Sc. and M.Sc. degrees in electrical engineering from Aswan University, Aswan, Egypt, in 2009 and 2013, respectively. In 2019, he received the Ph.D. degree from the Doctoral School of Electrical Engineering, Faculty of Electrical Engineering and informatics, Budapest University of Technology and Economics, Budapest, Hungary. Since 2010, he has been an assistant lecturer with the Faculty of Engineering, South Valley University (SVU), Qena, Egypt. He is currently working as an Assistant Professor with SVU. His research interests include modeling, analysis, control, and optimization of distribution systems with renewable energy sources and electric vehicles.

Bálint Hartmann received the M.Sc. degree in electrical engineering and the Ph.D. degree from Budapest University of Technology and Economics, in 2008 and 2013, respectively. He is an Associate Professor with the Department of Electric Power Engineering, Budapest University of Technology and Economics, Budapest, Hungary. He is also a part-time research fellow with the Centre for Energy Research, Hungarian Academy of Sciences, Budapest, Hungary. His research interests include the role of energy storage in power system, computer modelling and simulation of distribution networks and integration of variable renewable energy sources.